Phase ordering dynamics in binary mixtures with annealed vacancies

Sanjay Puri[1,2,3] and Radhika Sharma[1]
[1]School of Physical Sciences, Jawaharlal Nehru University, New Delhi 110 067, India
[2]Beckman Institute, 405 North Matthews Avenue, University of Illinois at Urbana–Champaign, Urbana, Illinois 61801-3080
[3]Department of Theoretical Physics, University of Manchester, Manchester M13 9PL, United Kingdom

(Received 27 November 1996; revised manuscript received 23 September 1997)

We formulate mean-field dynamical models for phase ordering dynamics in binary mixtures with both mobile and quenched vacancies or impurities. We use these models to obtain numerical results for two important problems in phase ordering dynamics, viz., the kinetics of vacancy-mediated segregation and the kinetics of ordering in a ferromagnet with annealed vacancies. [S1063-651X(98)01102-7]

PACS number(s): 64.70.−p

I. INTRODUCTION

Two-phase mixtures can exist in either a homogeneous state (at high temperatures) or an ordered state (at low temperatures), where the system separates into domains rich in one or the other constituent of the mixture. When a two-phase mixture in the homogeneous state is quenched below its critical temperature, it evolves towards the ordered state and the dynamics of this evolution is referred to as ''phase ordering dynamics'' [1]. The study of phase ordering dynamics has evoked much research interest and there have been many experimental, numerical, and analytical studies of this problem [1]. For pure and isotropic systems, it is now well established that the coarsening domains exhibit a morphological self-similarity in time and are characterized by a time-dependent length scale $L(t)$. This characteristic length scale exhibits a power-law behavior in time, i.e., $L(t)\sim t^{\phi}$, where t is the time and ϕ is referred to as the growth exponent. The functional form of the scaled structure factor, which characterizes the domain morphology [2], and the value of ϕ depend critically on whether or not the order parameter is conserved.

Most numerical studies of phase ordering dynamics start with microscopic models or their coarse-grained counterparts. At the microscopic level, the case with nonconserved order parameter (e.g., the ordering of a ferromagnet) is studied via Monte Carlo (MC) models, which associate Glauber spin-flip kinetics with a two-state Ising model. In these models, a spin S_i at a site i corresponds to an ''up'' or ''down'' state and can be flipped at random because there is no constraint on the order parameter, which is the local magnetization. The case with conserved order parameter (e.g., the segregation of a binary alloy AB) is complicated by a conservation constraint on the order parameter, which is the local difference in densities of A and B atoms. Any reasonable dynamical model must respect the fact that the numbers of A and B atoms are unchanged in time. This is usually mimicked at the microscopic level by associating Kawasaki spin-exchange kinetics [3] with a two-state Ising model. In this case, the spin variable S_i describes whether a site i is occupied by an A or a B atom.

At the phenomenological level, phase ordering dynamics is usually modeled in terms of partial differential equations. Thus the case with a nonconserved order parameter (NCOP) is modeled by the time-dependent Ginzburg-Landau (TDGL) equation

$$\frac{\partial\psi(\vec{r},t)}{\partial t}=-\frac{\delta H[\psi(\vec{r},t)]}{\delta\psi(\vec{r},t)}, \tag{1}$$

where $\psi(\vec{r},t)$ is the order parameter (spontaneous magnetization in the case of a ferromagnet) at point $\vec{r}$ and time t, and $H[\psi(\vec{r},t)]$ is an appropriate free-energy functional, usually taken to be of the ϕ^4 form. The case with a conserved order parameter (COP) is modeled by the Cahn-Hilliard (CH) equation [4]

$$\frac{\partial\psi(\vec{r},t)}{\partial t}=\nabla^2\left[\frac{\delta H[\psi(\vec{r},t)]}{\delta\psi(\vec{r},t)}\right], \tag{2}$$

where conservation is imposed by associating an extra $-\nabla^2$ operator with the chemical potential in Eq. (1). Thermal noise terms can also be introduced into Eqs. (1) and (2), but are not necessary as it has been demonstrated that the effects of thermal noise are irrelevant for the asymptotic behavior of phase ordering [5]. Equations (1) and (2) should be treated as purely phenomenological models and are not rigorously derivable from microscopic models. However, they can be motivated from appropriate microscopic models (i.e., the two-state Ising model with Glauber or Kawasaki kinetics) via a master equation approach in conjunction with the mean-field approximation [6].

At present, most well-established results for phase ordering systems have been obtained in the context of pure and isotropic systems. Of course, real experimental systems are neither pure nor isotropic. Recent interest in this area has focused on incorporating experimentally relevant effects into models of phase ordering dynamics. In particular, there have been a large number of studies of the effects of both quenched [7–9] and annealed [10–15] disorder on the dynamics of domain growth.

Quenched impurities trap growing domains and drastically alter the asymptotic domain growth law in a manner that is not yet fully understood [7,8]. However, the morphology of coarsening domains is unaffected by the presence of quenched disorder (other than in the case with random fields [9]) and the functional form of the scaled structure factor is independent of the amplitude of quenched disorder, a property that has been referred to as ''superuniversal scaling.''

Annealed impurities are relevant in two important classes of systems, viz., binary mixtures with surfactants (e.g., microemulsions) and binary mixtures with vacancies or impurities. There have been a number of studies of phase ordering in binary mixtures with surfactants [10,11]. There is a good understanding (at least numerically) of the functional form of the scaled structure factor, which again appears to be unaffected by the presence of surfactants. However, the asymptotic domain growth law is substantially altered and, to the best of our knowledge, there is still no consensus on the functional form of the asymptotic growth law.

In a recent paper, we have initiated a study of phase ordering dynamics with annealed vacancies [16]. In the present paper we expand the scope of this study and present detailed results for phase ordering dynamics in binary mixtures AB with annealed vacancies. There have been a number of previous studies of this problem [12–15] and we briefly review extant results here. Two classes of systems have been considered, viz., the ordering of ferromagnets with annealed vacancies, the NCOP case, and the segregation of binary mixtures with annealed vacancies, the COP case. Of course, it should be kept in mind that the vacancy field in both cases constitutes an additional order parameter, which is conserved.

Srolovitz and Hassold [12] conducted a MC study of diffusing impurities (e.g., vacancies) on domain growth in the NCOP case. They found that the vacancies tended to migrate to the interfacial regions. This leads to a dynamical crossover in the domain growth law from $L(t) \sim t^{1/2}$ [known as the Lifshitz-Cahn-Allen (LCA) law] in the early stages to a slower, nonalgebraic growth in the late stages. However, they did not examine the scaling behavior of the structure factor. Mouritsen and Shah [12] also investigated a similar model (though with antiferromagnetic interactions) and arrived at similar conclusions. A recent MC study of the NCOP case with a single vacancy was conducted by Vives and Planes [12]. In their model, dynamics is introduced via vacancy exchanges with the A or B atoms of a binary mixture with antiferromagnetic interactions. They find the somewhat puzzling result that the growth law is faster than the LCA law, a possible consequence of allowing vacancy exchanges with next-nearest-neighbor sites also.

At the coarse-grained level, the NCOP case can be described in terms of coupled dynamical equations for two order parameters: one for the ordering field, which is nonconserved; and the other for the vacancy field, which is conserved. In the classification of Hohenberg and Halperin [17], this is referred to as model C. Models in this category have been numerically simulated by Ohta *et al.* [13] and analytically studied by Elder *et al.* [13].

The COP case is considerably more interesting because vacancies play a critical role in phase separation dynamics. It is well known to materials scientists that Kawasaki exchange kinetics, which involves the direct interchange of A and B atoms in an AB mixture, is energetically unrealistic. As a matter of fact, it is believed that phase separation in binary alloys is mediated by vacancies [18]. Thus, in the context of binary alloys, vacancies do not merely serve as experimental complications in phase separation studies. Rather, they are a crucial factor in the dynamics of segregation. Vacancy-mediated phase separation was studied by Yaldram and Binder [14] via MC studies of a three-state spin model. Their studies demonstrated that the vacancies tended to cluster in the interfacial regions. Furthermore, they found that the qualitative behavior of vacancy-mediated segregation is similar to that for the usual direct-exchange mechanism. However, they did not make a quantitative comparison and also did not investigate the intermediate- or late-stage behavior. A more recent MC study is due to Fratzl and Penrose [14], who considered segregation in an AB mixture mediated by a single vacancy. These authors discovered the surprising result that domain growth mediated by a single vacancy is much faster than that for the usual direct-exchange mechanism. Moreover, the asymptotic domain growth in their study is consistent with the usual Lifshitz-Slyozov (LS) growth law for phase separation in binary mixtures, viz., $L(t) \sim t^{1/3}$. Before we proceed, it is worth pointing out that the Vives-Planes [12] and Fratzl-Penrose [14] models are in the same static universality class as the usual two-state Ising model for binary mixtures. This is because a single vacancy does not play a relevant role in the thermodynamic limit.

In this paper we formulate mean-field dynamical models for phase ordering in binary mixtures with mobile vacancies. We pursue two primary goals in this paper. The first is to provide a systematic phenomenological treatment of phase ordering dynamics in ternary (ABV) mixtures, with vacancies (denoted by V) acting as a third component in the mixture. Our second goal is to use these mean-field dynamical models to obtain detailed numerical results for the two problems that we have discussed above. In recent work, Plapp and Gouyet [15] have used similar mean-field dynamical models for ABV mixtures to investigate surface instabilities for droplets of the unstable mixture immersed in a stable vapor of the mixture.

This paper is organized as follows. In Sec. II, we present the model Hamiltonian for the ABV system and its mean-field solution. We also formulate mean-field dynamical models for vacancy-mediated phase separation and ordering of ferromagnets with vacancies. Section III contains detailed numerical results for the problem of vacancy-mediated phase separation. In Sec. IV, we present numerical results for the dynamics of ordering in a ferromagnet with annealed vacancies. Section V ends this paper with a summary and discussion of our results.

II. MEAN-FIELD DYNAMICAL MODELS FOR PHASE ORDERING DYNAMICS WITH VACANCIES

Consider a lattice model in which each site i can be occupied by either an A, a B, or a V ''atom.'' This model is applicable to both ternary (ABV) mixtures and ferromagnets with vacancies. In the latter context, A and B can be interpreted as up- and down-spin states, respectively. We assume that there is only a nearest-neighbor interaction and the energies associated with A-A, B-B, and A-B pairs are ϵ_{AA}, ϵ_{BB}, and ϵ_{AB}, respectively [14(a)]. We further assume that there is no interaction energy for pairs with at least one V atom. Then we can write the energy of the system in terms of a spin-1 model with the Hamiltonian

$$H=\frac{\epsilon_{AA}+\epsilon_{BB}-2\epsilon_{AB}}{4}\sum_{\langle ij\rangle} S_iS_j+\frac{\epsilon_{AA}-\epsilon_{BB}}{4}\sum_{\langle ij\rangle} (S_i^2S_j+S_iS_j^2)$$
$$+\frac{\epsilon_{AA}+\epsilon_{BB}+2\epsilon_{AB}}{4}\sum_{\langle ij\rangle} S_i^2S_j^2, \tag{3}$$

where $S_i=1$, 0, or -1 corresponds to an A, a V, or a B atom at site i, respectively. We consider the case $\epsilon_{AA}=\epsilon_{BB}=-\epsilon$, so that there is an attractive interaction between identical atoms. Then our Hamiltonian reduces to

$$H=-J\sum_{\langle ij\rangle} S_iS_j+K\sum_{\langle ij\rangle} S_i^2S_j^2, \tag{4}$$

where $J=(\epsilon+\epsilon_{AB})/2$ and $K=(\epsilon_{AB}-\epsilon)/2$. The Hamiltonian in Eq. (4) is a special case of the well-known Blume-Emery-Griffiths (BEG) model [19] and is known to exhibit a rich phase diagram. In general, the BEG Hamiltonian should also include terms involving fields that couple linearly with S_i (viz., $-h\Sigma_iS_i$) and S_i^2 (viz., $-\Delta\Sigma_iS_i^2$). We will investigate the dynamics of phase ordering in this model.

The mean-field solution for the model in Eq. (4) (at temperature T) is easily obtained [20] as

$$\langle S_k\rangle^s=\langle S_k^2\rangle^s \tanh\left[\frac{J}{T}\sum_{L_k} \langle S_{L_k}\rangle^s\right],$$

$$\langle S_k^2\rangle^s=\frac{2\cosh\left[\frac{J}{T}\sum_{L_k}\langle S_{L_k}\rangle^s\right]}{2\cosh\left[\frac{J}{T}\sum_{L_k}\langle S_{L_k}\rangle^s\right]+\exp\left[\frac{K}{T}\sum_{L_k}\langle S_{L_k}^2\rangle^s\right]}, \tag{5}$$

where L_k refers to the neighbors of site k and we have set the Boltzmann constant to unity. Nonzero external fields h and Δ are trivially incorporated in Eq. (5). In Eq. (5) we use the superscript s to label the static solution. There are two order parameters, viz., $\langle S_k\rangle^s$, which refers to the AB field, and $\langle S_k^2\rangle^s$ (or $1-\langle S_k^2\rangle^s$), which refers to the vacancy field. These order parameters are not independent of each other. The static, homogeneous solutions of Eq. (5) arise from

$$S^*=\frac{2\sinh\left[\frac{qJ}{T}S^*\right]}{2\cosh\left[\frac{qJ}{T}S^*\right]+\exp\left[\frac{qK}{T}P^*\right]},$$

$$P^*=\frac{2\cosh\left[\frac{qJ}{T}S^*\right]}{2\cosh\left[\frac{qJ}{T}S^*\right]+\exp\left[\frac{qK}{T}P^*\right]}, \tag{6}$$

where $S^*=\langle S\rangle$, $P^*=\langle S^2\rangle$, and q is the number of nearest neighbors of a site.

In our discussion below, we focus on the case $K=0$ (i.e., $\epsilon_{AB}=-\epsilon_{AA}=-\epsilon_{BB}$), which corresponds to the spin-1 Ising model, as this simplifies our calculations considerably. Of course, the approach we formulate below generalizes to the $K\neq 0$ case in a straightforward fashion and we will also present models for $K\neq 0$.

For the case $K=0$, the only solution of Eq. (6) for $T>T_c$ $(=2qJ/3)$ is $S^*=0$, $P^*=2/3$, corresponding to the disordered state. For $T<T_c$, an ordered solution with $S^*\neq 0$ emerges, corresponding to a separation into A- and B-rich regions. The introduction of nonzero K and fields h,Δ considerably enriches the phase diagram [19]. We do not go into the details of the complete phase diagram here but will merely use relevant information wherever necessary.

A. Vacancy-mediated segregation in the *ABV* model

We first consider the physically relevant situation where the microscopic stochastic dynamics associated with the ABV Hamiltonian consists of nearest-neighbor spin exchanges, but only between A-V $(1\leftrightarrow 0)$ and B-V $(-1\leftrightarrow 0)$. We do not permit energetically unrealistic A-B (Kawasaki) exchanges. The master equation that describes this stochastic dynamics for a system of N spins is

$$\frac{\partial}{\partial t}P(S_1,\ldots,S_i,S_{L_i},\ldots,S_N;t)$$
$$=-\sum_i\sum_{L_i} W(S_i\leftrightarrow S_{L_i})[1+S_iS_{L_i}]$$
$$\times P(S_1,\ldots,S_i,S_{L_i},\ldots,S_N;t)$$
$$+\sum_i\sum_{L_i} W(S_{L_i}\leftrightarrow S_i)[1+S_iS_{L_i}]$$
$$\times P(S_1,\ldots,S_{L_i},S_i,\ldots,S_N;t). \tag{7}$$

In Eq. (7), $P(S_1,\ldots,S_i,\ldots,S_N;t)$ is the time-dependent probability distribution for a spin configuration $\{S_i\}$. The first term on the right-hand side corresponds to transitions out of the spin configuration $\{S_i\}$ via spin exchanges $S_i\leftrightarrow S_{L_i}$. The factor $[1+S_iS_{L_i}]$ enforces the constraint that only transitions of the type $\pm 1\leftrightarrow 0$ are permitted. The functional form of the transition probability is chosen to be consistent with the detailed balance condition, viz.,

$$W(S_i\leftrightarrow S_j)=\frac{1}{2\tau_1}\left[1-\tanh\left(\frac{\Delta H(S_i\leftrightarrow S_j)}{2T}\right)\right], \tag{8}$$

where we associate a time scale of τ_1 with a spin-exchange process and $\Delta H(S_i\leftrightarrow S_j)$ is the change in energy associated with the microscopic process. For simplicity of presentation, we initially confine ourselves to the case $K=0$ and later present results for $K\neq 0$. Then we have

$$\Delta H(S_i\leftrightarrow S_j)=J\sum_{L_i\neq j} (S_i-S_j)S_{L_i}-J\sum_{L_j\neq i} (S_i-S_j)S_{L_j}. \tag{9}$$

We multiply both sides of the master equation by S_k and perform a configuration average to obtain (after some algebra)

$$\tau_1 \frac{\partial \langle S_k \rangle}{\partial t} = -\sum_{L_k} \langle S_k(1-S_{L_k}^2) - S_{L_k}(1-S_k^2)\rangle + \sum_{L_k} \left\langle [1+S_k S_{L_k}](S_k - S_{L_k})^2 \tanh\left[\frac{J}{2T}\left(\sum_{L_k} S_{L_k} - \sum_{L_{L_k}} S_{L_{L_k}}\right)\right]\right\rangle$$
$$= -q\langle S_k\rangle + \sum_{L_k} \langle S_{L_k}\rangle - \sum_{L_k} \langle S_k^2 S_{L_k} - S_k S_{L_k}^2\rangle + \sum_{L_k} \left\langle (S_k^2 + S_{L_k}^2 - 2S_k^2 S_{L_k}^2)\tanh\left[\frac{J}{2T}\left(\sum_{L_k} S_{L_k} - \sum_{L_{L_k}} S_{L_{L_k}}\right)\right]\right\rangle . \tag{10}$$

So far, we have made no simplifying approximations and our dynamical equations are exact within the framework of our model. Equation (10) is part of an infinite hierarchy of coupled equations, which are intractable. It is customary to simplify this exact (but intractable) system of equations by invoking a mean-field (MF) approximation, which yields

$$\tau_1 \frac{\partial \langle S_k \rangle}{\partial t} = -q\langle S_k\rangle + \sum_{L_k} \langle S_{L_k}\rangle - \sum_{L_k} (\langle S_k^2\rangle\langle S_{L_k}\rangle - \langle S_k\rangle\langle S_{L_k}^2\rangle) + \sum_{L_k} (\langle S_k^2\rangle + \langle S_{L_k}^2\rangle - 2\langle S_k^2\rangle\langle S_{L_k}^2\rangle)$$
$$\times \tanh\left[\frac{J}{2T}\left(\sum_{L_k} \langle S_{L_k}\rangle - \sum_{L_{L_k}} \langle S_{L_{L_k}}\rangle\right)\right]. \tag{11}$$

In similar fashion, we can obtain a dynamical equation for $\langle S_k^2\rangle$ by multiplying the master equation with S_k^2 and configuration averaging to obtain (again after some algebra)

$$\tau_1 \frac{\partial \langle S_k^2 \rangle}{\partial t} = -\sum_{L_k} \langle (S_k^2 - S_{L_k}^2)(1+S_k S_{L_k})\rangle + \sum_{L_k} \left\langle [1+S_k S_{L_k}](S_k^2 - S_{L_k}^2)(S_k - S_{L_k})\tanh\left[\frac{J}{2T}\left(\sum_{L_k} S_{L_k} - \sum_{L_{L_k}} S_{L_{L_k}}\right)\right]\right\rangle . \tag{12}$$

Now notice that

$$(S_k^2 - S_{L_k}^2)(1+S_k S_{L_k}) = S_k^2 - S_{L_k}^2,$$
$$[1+S_k S_{L_k}](S_k^2 - S_{L_k}^2)(S_k - S_{L_k}) = S_k + S_{L_k} - S_k^2 S_{L_k} - S_k S_{L_k}^2, \tag{13}$$

where we have used the fact that $S_k^3 = S_k$. Then Eq. (12) simplifies to

$$\tau_1 \frac{\partial \langle S_k^2 \rangle}{\partial t} = -q\langle S_k^2\rangle + \sum_{L_k} \langle S_{L_k}^2\rangle + \sum_{L_k} \left\langle (S_k + S_{L_k} - S_k^2 S_{L_k} - S_k S_{L_k}^2)\tanh\left[\frac{J}{2T}\left(\sum_{L_k} S_{L_k} - \sum_{L_{L_k}} S_{L_{L_k}}\right)\right]\right\rangle . \tag{14}$$

Finally, we invoke the MF approximation to obtain the required dynamical equation

$$\tau_1 \frac{\partial \langle S_k^2 \rangle}{\partial t} = -q\langle S_k^2\rangle + \sum_{L_k} \langle S_{L_k}^2\rangle + \sum_{L_k} (\langle S_k\rangle + \langle S_{L_k}\rangle - \langle S_k\rangle\langle S_{L_k}^2\rangle - \langle S_k^2\rangle\langle S_{L_k}\rangle)\tanh\left[\frac{J}{2T}\left(\sum_{L_k} \langle S_{L_k}\rangle - \sum_{L_{L_k}} \langle S_{L_{L_k}}\rangle\right)\right]. \tag{15}$$

Equations (11) and (15) constitute our MF dynamical model for phase separation mediated by vacancies. It is easy to confirm that the spatial integrals of both order parameters are conserved. Furthermore, if we start off with an initial condition in which there are no vacancies (i.e., $\langle S_k^2\rangle = 1$ everywhere) or all vacancies (i.e., $\langle S_k\rangle = \langle S_k^2\rangle = 0$ everywhere), there is no dynamics at all and Eqs. (11) and (15) trivially reduce to

$$\tau_1 \frac{\partial \langle S_k^n \rangle}{\partial t} = 0, \quad n = 1,2. \tag{16}$$

We can retrace the steps in our calculation above to obtain the appropriate MF dynamical model for $K \neq 0$. This model takes the form

$$\tau_1 \frac{\partial \langle S_k \rangle}{\partial t} = -q\langle S_k\rangle + \sum_{L_k} \langle S_{L_k}\rangle - \sum_{L_k} (\langle S_k^2\rangle\langle S_{L_k}\rangle - \langle S_k\rangle\langle S_{L_k}^2\rangle) + \frac{1}{2}\sum_{n=1,2} (-1)^n \sum_{L_k} [\langle S_k\rangle + \langle S_{L_k}\rangle + (-1)^n\langle S_k^2\rangle + (-1)^n\langle S_{L_k}^2\rangle$$
$$- \langle S_k^2\rangle\langle S_{L_k}\rangle - \langle S_k\rangle\langle S_{L_k}^2\rangle - (-1)^n 2\langle S_k^2\rangle\langle S_{L_k}^2\rangle]\tanh\left[\frac{J}{2T}\left(\sum_{L_k} \langle S_{L_k}\rangle - \sum_{L_{L_k}} \langle S_{L_{L_k}}\rangle\right)\right.$$
$$\left. - (-1)^n \frac{K}{2T}\left(\sum_{L_k} \langle S_{L_k}^2\rangle - \sum_{L_{L_k}} \langle S_{L_{L_k}}^2\rangle\right)\right] \tag{17}$$

and

$$\tau_1 \frac{\partial\langle S_k^2\rangle}{\partial t} = -q\langle S_k^2\rangle + \sum_{L_k} \langle S_{L_k}^2\rangle + \frac{1}{2}\sum_{n=1,2}\sum_{L_k} [\langle S_k\rangle + \langle S_{L_k}\rangle + (-1)^n\langle S_k^2\rangle + (-1)^n\langle S_{L_k}^2\rangle - \langle S_k^2\rangle\langle S_{L_k}\rangle - \langle S_k\rangle\langle S_{L_k}^2\rangle - (-1)^n 2\langle S_k^2\rangle \times\langle S_{L_k}^2\rangle]\tanh\left[\frac{J}{2T}\left(\sum_{L_k}\langle S_{L_k}\rangle - \sum_{L_{L_k}}\langle S_{L_{L_k}}\rangle\right) - (-1)^n\frac{K}{2T}\left(\sum_{L_k}\langle S_{L_k}^2\rangle - \sum_{L_{L_k}}\langle S_{L_{L_k}}^2\rangle\right)\right]. \tag{18}$$

Finally, for completeness, we also present the mean-field dynamical model that arises for the corresponding nonconserved dynamics. In the nonconserved case, we only allow spontaneous transitions of the spin variable S_i from $\pm 1 \rightarrow 0$ (or vice versa) on a time scale τ_2. Of course, the $S_i = 0$ state in this model can no longer be associated with vacancies as the number of vacancies must be conserved. The appropriate mean-field dynamical model for the nonconserved case is

$$2\tau_2 \frac{\partial\langle S_k\rangle}{\partial t} = -\langle S_k\rangle + \sum_{n=1,2}\left(\frac{2+(-1)^n\langle S_k\rangle - \langle S_k^2\rangle}{2}\right)\tanh\left[\frac{J}{2T}\sum_{L_k}\langle S_{L_k}\rangle - (-1)^n\frac{K}{2T}\sum_{L_k}\langle S_{L_k}^2\rangle\right] \tag{19}$$

and

$$2\tau_2 \frac{\partial\langle S_k^2\rangle}{\partial t} = 2 - 3\langle S_k^2\rangle + \sum_{n=1,2}(-1)^n\left(\frac{2+(-1)^n\langle S_k\rangle - \langle S_k^2\rangle}{2}\right)\tanh\left[\frac{J}{2T}\sum_{L_k}\langle S_{L_k}\rangle - (-1)^n\frac{K}{2T}\sum_{L_k}\langle S_{L_k}^2\rangle\right]. \tag{20}$$

We can demonstrate by direct substitution that the static solutions in Eq. (5) are explicitly contained in Eqs. (17)–(20). The algebra is straightforward, though somewhat involved, and we do not present it here. Furthermore, we can also obtain coupled nonlinear partial differential equations equivalent to our MF dynamical models by identifying the order parameters $\langle S_k\rangle \equiv \psi(\vec{r},t)$ and $\langle S_k^2\rangle \equiv \phi(\vec{r},t)$. We do not present these equations here as the numerical results reported later are obtained by directly simulating the MF dynamical models presented above.

Before we proceed to the next section, we would like to discuss the nature of our modeling via MF dynamical models. Our models are macroscopic-level descriptions of the microscopic dynamical models that were our starting point. The transition to a coarse-grained level of description is implicit in the configuration averaging in conjunction with the MF approximation. Nevertheless, we expect our macroscopic models to be in the same dynamical universality class as the underlying microscopic models. Furthermore, as a consequence of the smoothening inherent in our coarse-graining procedure, we expect our macroscopic models to constitute a far more reliable and convenient means of accessing the asymptotic behavior of phase ordering dynamics, especially in the COP case. It is well known that, in spite of extensive numerical efforts, MC models of phase separation in pure binary mixtures [21] are still unable to access the true asymptotic regime in which the characteristic domain size obeys the LS growth law $L(t) \sim t^{1/3}$. On the other hand, at least for pure binary mixtures, the asymptotic behavior is easily accessed using phenomenological cell dynamical system models [22,23] and MF dynamical models [11(b)] of the kind discussed here.

The second point we wish to address concerns the deterministic nature of our models. We can incorporate the effects of thermal fluctuations in our deterministic models and thereby obtain mesoscopic-level models [24]. However, in the pure case, thermal noise has been demonstrated to be asymptotically irrelevant [5]. Physically, this is a consequence of the fact that thermal noise affects interfaces on a fixed length scale, which becomes progressively irrelevant in comparison to the growing domain length scales. We expect a similar argument to apply here also. Thus it is reasonable and convenient to work with deterministic models, at least in the context of late-stage behavior.

B. Ordering of ferromagnets with annealed vacancies

We next consider the phase ordering dynamics of ferromagnets with annealed vacancies. In this case, there are two mechanisms whereby the system evolves, i.e., (a) microscopic spin-flip processes, with S_i flipping from $1 \rightarrow -1$ and vice versa, and (b) exchange of spins ($S_i = \pm 1$) with vacancies, as in the preceding subsection. We have already formulated a mean-field dynamical model for the conserved dynamics of (b) in the preceding subsection. We now specify the model corresponding to the nonconserved process of (a). The spins with value 0 (representing vacancies) do not play a role in the nonconserved dynamics but act as trapping sites for coarsening domains. Therefore, the impurity field $\langle S_k^2\rangle$ has no dynamical evolution in the context of spin-flip processes and merely plays the role of quenched disorder.

The master equation that describes spin-flip dynamics for a system of N spins is

$$\frac{\partial}{\partial t}P(S_1,\ldots,S_i,\ldots,S_N;t) = -\sum_i W(S_i \rightarrow -S_i)P(S_1,\ldots,S_i,\ldots,S_N;t) + \sum_i W(-S_i \rightarrow S_i)P(S_1,\ldots,-S_i,\ldots,S_N;t), \tag{21}$$

where the various quantities have the same meaning as before. The transition probability $W(S_i \rightarrow -S_i)$ has the usual form

$$W(S_i \rightarrow -S_i) = \frac{1}{2\tau_3}\left(1 - \tanh\left[\frac{\Delta H(S_i \rightarrow -S_i)}{2T}\right]\right), \quad (22)$$

where τ_3 is a characteristic time scale for the spin-flip process. In this case we have

$$\Delta H(S_i \rightarrow -S_i) = 2JS_i \sum_{L_i} S_{L_i}, \quad (23)$$

which is valid for arbitrary K. This is because the vacancies are unaffected by the microscopic dynamics and the second term in the ABV Hamiltonian stays unchanged.

We next multiply both sides of the master equation by S_k and perform a configurational average to obtain

$$\tau_3 \frac{\partial \langle S_k \rangle}{\partial t} = -\langle S_k \rangle + \left\langle S_k^2 \tanh\left[\frac{J}{T}\sum_{L_k} S_{L_k}\right]\right\rangle. \quad (24)$$

Finally, we invoke the MF approximation to obtain the dynamical model

$$\tau_3 \frac{\partial \langle S_k \rangle}{\partial t} = -\langle S_k \rangle + \langle S_k^2 \rangle \tanh\left[\frac{J}{T}\sum_{L_k} \langle S_{L_k} \rangle\right]. \quad (25)$$

It is easy to verify that

$$\tau_3 \frac{\partial \langle S_k^2 \rangle}{\partial t} = 0, \quad (26)$$

as is apparent from the microscopic dynamics. It is also obvious that Eq. (25) contains the static solution for $\langle S_k \rangle$ from Eq. (5).

It is instructive to identify the order parameter fields $\langle S_k \rangle \equiv \psi(\vec{r},t)$ and $\langle S_k^2 \rangle \equiv \phi(\vec{r})$ in Eq. (25). We Taylor expand terms in the argument of the tanh function and then perform a small-argument expansion of the tanh function. This procedure yields the nonlinear partial differential equation equivalent to Eq. (25),

$$\tau_3 \frac{\partial \psi(\vec{r},t)}{\partial t} = \left[\frac{qJ}{T}\phi(\vec{r}) - 1\right]\psi(\vec{r},t) - \frac{1}{3}\left(\frac{qJ}{T}\right)^3 \phi(\vec{r})\psi(\vec{r},t)^3 + \frac{Ja^2}{T}\phi(\vec{r})\nabla^2\psi(\vec{r},t), \quad (27)$$

where a is the lattice spacing. Thus quenched vacancies (impurities) have the effect of randomizing the coefficients of the TDGL equation for the nonconserved case [25,8]. The desired mean-field dynamical model for ordering in ferromagnets with vacancies is obtained by combining terms in Eqs. (25) and (26) with terms in Eqs. (17) and (18), respectively.

Finally, for completeness, we consider the case where A and B are allowed to interchange (i.e., Kawasaki kinetics) and the vacancies or impurities act as quenched disorder. The resultant mean-field dynamical model is

$$\tau_4 \frac{\partial \langle S_k \rangle}{\partial t} = \sum_{L_k} (\langle S_k^2 \rangle \langle S_{L_k} \rangle - \langle S_k \rangle \langle S_{L_k}^2 \rangle) - \sum_{L_k} (\langle S_k \rangle \langle S_{L_k} \rangle - \langle S_k^2 \rangle \langle S_{L_k}^2 \rangle) \tanh\left[\frac{J}{T}\left(\sum_{L_k} \langle S_{L_k} \rangle - \sum_{L_{L_k}} \langle S_{L_{L_k}} \rangle\right)\right] \quad (28)$$

and

$$\tau_4 \frac{\partial \langle S_k^2 \rangle}{\partial t} = 0, \quad (29)$$

where τ_4 is the time scale of the microscopic dynamics. It is again obvious that the static solution from Eq. (5) is contained in Eq. (28). We can also coarse grain further to obtain the nonlinear partial differential equation corresponding to Eq. (28). At the phenomenological level, this is simply obtained by appending an extra $-\nabla^2$ operator to the chemical potential in Eq. (27) [8].

We will next present numerical results obtained from simulations of these models. In particular, Sec. III contains results from a simulation of phase separation mediated by vacancies. Section IV presents results from a simulation of ordering dynamics in a ferromagnet with annealed vacancies. In both cases, we directly simulate the appropriate MF dynamical models as these provide a convenient alternative to the partial differential equation models.

III. NUMERICAL RESULTS FOR VACANCY-MEDIATED PHASE SEPARATION

Our numerical results for vacancy-mediated phase separation were obtained using the MF dynamical models in Eqs. (11) and (15) (i.e., for $K=0$), with τ_1 scaled into the time variable. We simulated these coupled equations in two dimensions on a lattice of size N^2 using a simple Euler discretization scheme with mesh size $\Delta t = 0.01$. Periodic boundary conditions were applied in both directions. We confirmed that further reduction of the mesh size did not change our numerical results. The parameter values for our simulation were $K=0$ and $T=0.375T_c$. Results similar to those presented here are obtained for a wide range of temperature values with the only change being in the coefficients of growth laws.

The initial conditions for the $\langle S_k \rangle$ and $\langle S_k^2 \rangle$ fields in each run were chosen to be uniformly distributed random fluctuations about some background and mimicked the disordered homogeneous state before the quench. The background value was 0 for the $\langle S_k \rangle$ field, corresponding to an equal mix of A and B atoms. For the $\langle S_k^2 \rangle$ field, we considered background values $v_0 = 0.93$ and 0.96, corresponding to a rather high concentration of vacancies. We used these high concentrations as we were interested in investigating nonuniversal effects and/or different late-stage dynamics which may result because of the presence of vacancies.

We studied phase ordering in the ABV model using three tools: evolution pictures and order parameter profiles, the time-dependent structure factor for the AB field, and characteristic domain length scales. The time-dependent structure factor $S(\vec{k},t)$ for the AB field is defined as

$$S(\vec{k},t)=\langle \psi(\vec{k},t)\psi(\vec{k},t)^*\rangle, \tag{30}$$

where $\psi(\vec{k},t)$ is the discrete Fourier transform of the AB field ($\langle S_k\rangle$) with wave vector $\vec{k}$ and time t. In our discrete simulation, the wave vectors take values $\vec{k}=(2\pi/N)(n_x,n_y)$, where n_x and n_y range from $-N/2$ to $N/2-1$. The angular brackets in Eq. (30) refer to an averaging over independent initial conditions. In our simulations reported here, the structure factor is calculated for systems of size 256^2 as an average over 50 independent runs. As we have remarked earlier, an interesting aspect of phase ordering systems is the dynamical scaling of the time-dependent structure factor, i.e., the morphology of coarsening domains is unchanged in time. The dynamical scaling form of the structure factor for isotropic systems is

$$S(\vec{k},t)=L(t)^dF(kL(t)), \tag{31}$$

where d is the dimensionality and $F(x)$ is a time-independent master function. In our simulations, we spherically average the structure factor $S(\vec{k},t)$ to obtain the scalar structure factor $S(k,t)$, which we will present subsequently.

We define the characteristic length scale $L(t)$ as the reciprocal of the first moment of the spherically averaged structure factor, i.e., $L(t)=\langle k\rangle^{-1}$, where

$$\langle k\rangle=\frac{\int_0^{k_m}dk\ k\ S(k,t)}{\int_0^{k_m}dk\ S(k,t)}. \tag{32}$$

In Eq. (32), the upper cutoff k_m is taken as being half the magnitude of the largest wave vector lying in the Brillouin zone of our discrete lattice. We have confirmed that the structure factor has decayed sufficiently by this value so that a further increase in k_m does not affect the value of $\langle k\rangle$. The characteristic length scale can be defined in a number of ways, all of which are equivalent in the dynamical scaling regime [2].

Figure 1 shows an evolution picture obtained from our MF dynamical model for vacancy-mediated phase separation, implemented on a 128^2 lattice. The initial condition is as described above and the background vacancy field is $v_0=0.93$. Regions where $\langle S_k\rangle$ is positive (say, A rich) are marked in black and those where $\langle S_k\rangle$ is negative (B rich) are not marked. We interpret regions where $\langle S_k^2\rangle$ falls below 0.7 as being vacancy-rich and these are marked by crosses. There are two important features that emerge from these pictures. Firstly, vacancy-mediated segregation dynamics gives rise to a morphology that is similar to that obtained from the usual Kawasaki exchange in pure AB mixtures. Second, vacancies rapidly migrate to the interfacial regions as this is energetically favorable.

The static solutions for the phase separation problem (i.e., with fixed concentrations of A, B, and V) in the case $K=0$ correspond to two-phase coexistence, i.e., in equilibrium, there are A-rich and B-rich phases with a uniform vacancy field v_0, which is the same as that in the initial condition. The deviations from v_0 in the interfacial regions are irrelevant in the thermodynamic limit.

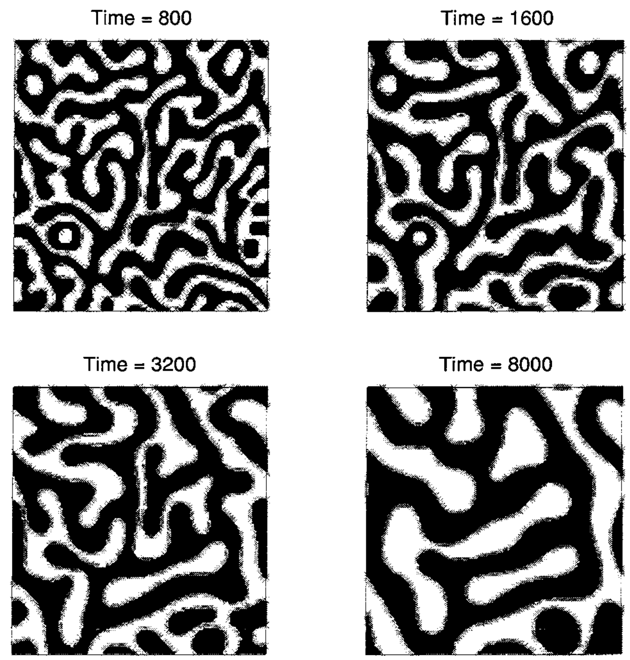

FIG. 1. Temporal evolution from a disordered initial condition for our mean-field dynamical model of vacancy-mediated phase separation in the ABV model with $K=0$. These pictures were obtained from a simple Euler discretization (with mesh size $\Delta t=0.01$) of Eqs. (11) and (15) (with τ_1 absorbed into the definition of time t) on a two-dimensional lattice of size 128^2. Periodic boundary conditions were imposed in both directions. The parameter value for this simulation was $T=0.375T_c$. The initial condition for the $\langle S_k\rangle$ (or AB) field consists of uniformly distributed small-amplitude fluctuations about a zero background, mimicking a homogeneous state. The initial condition for the $\langle S_k^2\rangle$ (or vacancy) field consists of similar fluctuations about a background $v_0=0.93$. Regions with positive $\langle S_k\rangle$ are marked in black and regions with negative $\langle S_k\rangle$ are not marked. Regions where $\langle S_k^2\rangle$ falls below 0.7 (i.e., vacancy rich) are marked as crosses and are confined to the interfacial regions, as is clear from the pictures. The dimensionless evolution times are specified above each frame.

However, there is a range of values of K where the model also exhibits three-phase coexistence, with the third phase corresponding to a V-rich phase. In this situation, the thickness of the vacancy layer at the interface increases with time because the overall interfacial area is diminished as the domains coarsen. This makes the surface tension time dependent and results in a slowing down (and possibly freezing) of domain growth. Similar effects are seen in the case of binary mixtures with surfactants [11]. We are presently investigating the dynamical evolution of the phase separating system in this parameter regime in greater detail.

Figure 2 shows the variation of the order-parameter fields along a specified cross section in the evolution pictures of Fig. 1. The cross section is parallel to the horizontal axis and midway up the vertical axis. The solid and dashed lines refer to the fields $\langle S_k\rangle$ and $\langle S_k^2\rangle$, respectively. It is evident from Fig. 2 that the vacancy concentration is maximum in the AB interfacial regions. Similar pictures are obtained for $v_0=0.96$ also and were presented in an earlier paper [16].

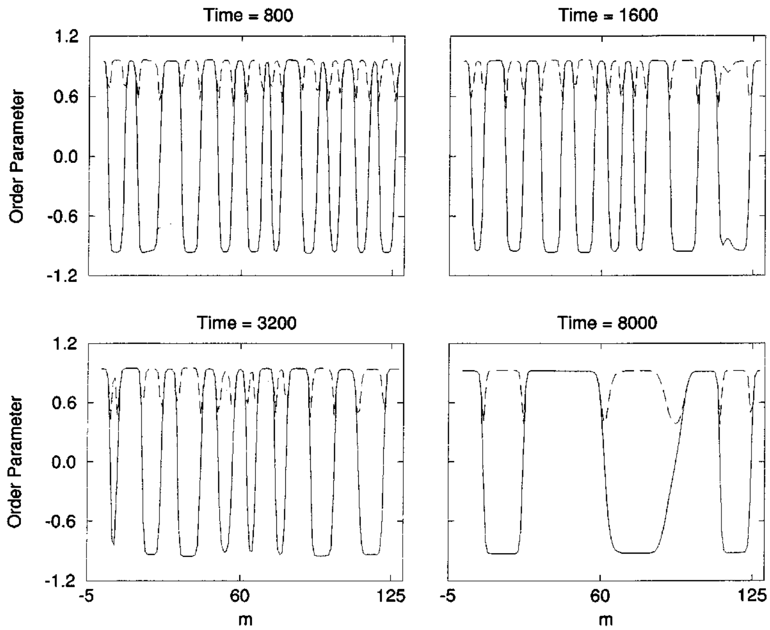

FIG. 2. Order parameter profiles corresponding to the evolution depicted in Fig. 1. The profiles are measured along a cross section parallel to the horizontal axis and located at the middle of the vertical axis. The solid line refers to the $\langle S_k \rangle$ (or AB) field and the dashed line refers to the $\langle S_k^2 \rangle$ (or V) field.

Figure 3 tests the dynamical scaling of the time-dependent structure factor for the temporal evolution depicted in Fig. 1. Figure 3(a) superposes data for $S(k,t)\langle k \rangle^2$ vs $k/\langle k \rangle$ from dimensionless times 1600, 4800, 6400, and 8000. The data from different times collapses onto a master curve reasonably well, except in the peak region, where there is still some drift. Figure 3(b) plots the data of Fig. 3(a) on a log-log scale and shows that the data collapse is good in the intermediate tail region also. The extreme tail region shows a slow upward drift, which we would like to discuss at some length here. In the pure case, where there are no vacancies, it is known that the finite interfacial thickness σ_W gives rise to nonuniversal effects in the tail [26]. As the domain size $L(t)$ increases, $\sigma_W/L(t) \rightarrow 0$ and the nonuniversal effects are pushed out to higher and higher values of the scaled wave vector $k/\langle k \rangle$. On the scaled plot analogous to Fig. 3(b) for the pure case, this is manifested as a marked upward drift in the tail of the structure factor. Asymptotically in time, the structure factor for the pure case exhibits the Porod tail $[S(k,t) \sim k^{-(d+1)}$ for large $k]$, which is associated with scattering off sharp interfaces [27].

In the present case, our data show only a weak upward drift in the tail. A possible reason for this is the extreme softness of vacancy-rich interfaces compared to interfaces in the pure case. Furthermore, as we will see later, domain growth is considerably slower in the vacancy-driven case. Nevertheless, even in the present case, we expect to recover Porod's law at sufficiently long times because the interfacial thickness does not grow with time. However, in the physical situation where we have a macroscopic vacancy-rich layer growing at the interface, the effective interface width is time dependent. From simple geometric considerations, we find that the thickness of the vacancy layer is proportional to $L(t)$. If we make the reasonable assumption that the interfacial thickness $\sigma_W(t)$ grows at the same rate as the thickness of the vacancy layer, $\sigma_W(t)/L(t) \simeq$ const. In such a situation, we would not expect to recover Porod's law even asymptotically in time.

Figure 4(a) compares the scaled structure factor for the pure case with spin-exchange dynamics and those for vacancy-mediated spinodal decomposition with $v_0 = 0.93$ and 0.96. Data for the pure case are obtained from a two-dimensional simulation of a MF dynamical model similar to that described previously. The parameter value for our simulation of the pure case is $T = 0.75T_c$, where T_c is the MF critical temperature of the Ising model. The scaled structure factors are in reasonable agreement, but appear to be slightly offset from each other. This is a possible consequence of the slow approach to asymptotic behavior in vacancy-mediated segregation dynamics. As a matter of fact, the scaled data for the case with $v_0 = 0.93$, corresponding to a higher vacancy concentration and faster domain growth, is somewhat closer to the pure case than the data for $v_0 = 0.96$. Figure 4(b) is a log-log plot of the data in Fig. 4(a) and highlights the difference between the scaled structure factors for the pure case and the vacancy-driven case. The characteristic shoulder in the scaled structure factor for the pure case at $k/\langle k \rangle \simeq 2.0$ appears to be absent in the vacancy-driven case. The extreme tail for the pure case also lies below the tails for the vacancy-driven case. However, with the passage of time, the extreme tails in all cases will rise and asymptotically approach the Porod tail [marked as a dashed line in Fig. 4(b)].

Finally, Fig. 5 studies the time dependence of the characteristic domain size $L(t) = \langle k \rangle^{-1}$. Figure 5(a) plots $L(t)$ vs t for the pure case (up to $t = 4000$) and the vacancy-driven cases with $v_0 = 0.93$ and 0.96 (up to $t = 8000$). We have used a nonlinear fitting routine to fit the length scale data to the functional form $L(t) = a + bt^{\phi}$ and the resultant best fits are denoted as solid lines on the data sets. The best-fit growth exponents are $\phi = 0.33 \pm 0.01$ for the pure case, $\phi = 0.34 \pm 0.01$ for $v_0 = 0.93$, and $\phi = 0.32 \pm 0.01$ for $v_0 = 0.96$. These are in excellent agreement with the LS growth law $L(t) \sim a + bt^{1/3}$. Figure 5(b) is a log-log plot of the data from Fig. 5(a) for the vacancy-driven cases. In this case, we fit the data by a straight line and the best-fit lines are superposed on the appropriate data sets. The slopes correspond to $\phi = 0.33 \pm 0.01$ for $v_0 = 0.93$ and $\phi = 0.32 \pm 0.01$ for $v_0 = 0.96$.

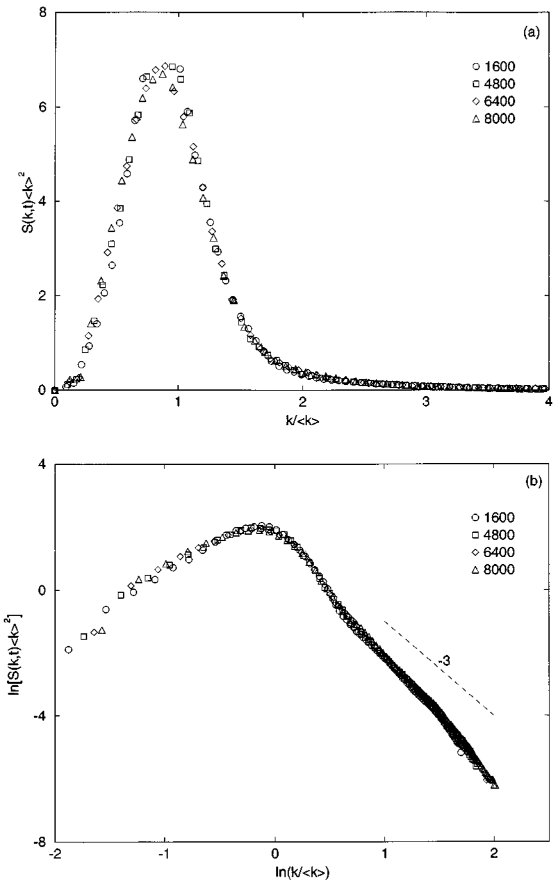

FIG. 3. (a) Scaled structure factors $S(k,t)\langle k\rangle^2$ vs $k/\langle k\rangle$ for the evolution depicted in Fig. 1. The structure factors are obtained on systems of size 256^2 as an average over 50 independent runs. We superpose data from dimensionless times 1600, 4800, 6400, and 8000 in the figure. (b) Data from (a), plotted on a log-log scale. The dashed line has a slope of -3 and refers to the two-dimensional (2D) Porod tail [i.e., $S(k,t)\sim k^{-3}$ for large k in two dimensions], which characterizes scattering off sharp interfaces.

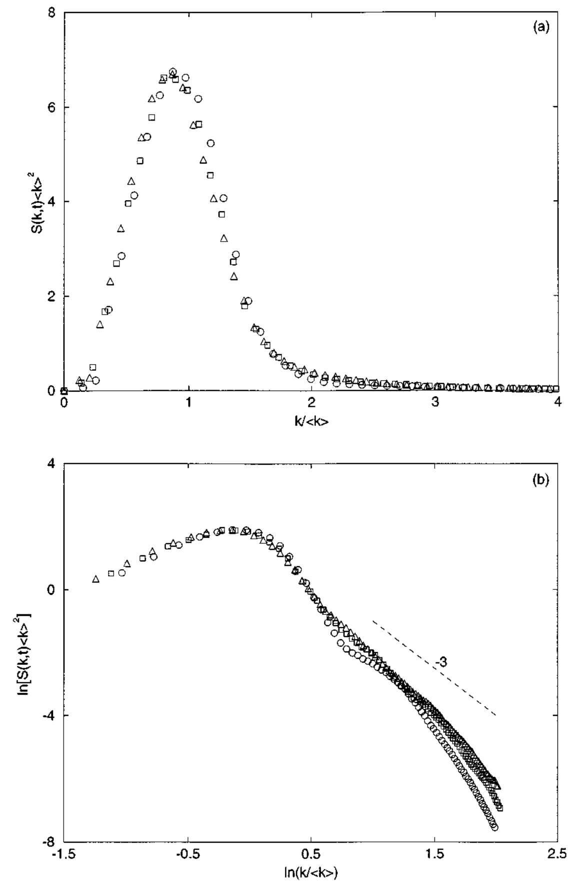

FIG. 4. (a) Comparison of scaled structure factors for the pure case (denoted by ○'s) and the vacancy-driven cases with $v_0=0.93$ (denoted by □'s) and $v_0=0.96$ (denoted by △'s). The data for the pure case is obtained using statistics similar to that for the vacancy-driven cases. Data for the pure case are from dimensionless time 4000 and for the vacancy-driven cases from dimensionless time 8000. (b) Data from (a), plotted on a log-log scale. Symbols have the same meaning as in (a). The dashed line refers to the 2D Porod tail, as in Fig. 3(b).

For parameter values that give rise to three-phase coexistence, the vacancy layer at the interface grows with the passage of time and the AB interfacial tension diminishes drastically. The time dependence of the interfacial tension results in considerably slower growth at late times [11] and we are presently studying this in greater detail.

IV. NUMERICAL RESULTS FOR ORDERING IN FERROMAGNETS WITH VACANCIES

We next consider the ordering of a ferromagnet with annealed vacancies. In the terminology of the ABV model, we permit spin flips from $1\rightarrow-1$ and vice versa with a time scale τ_3, as modeled by Eqs. (25) and (26). In conjunction with these spin flips, we consider spin exchanges $\pm1\leftrightarrow0$, so that a magnetic atom can move into a vacant site. We associate a time scale τ_1 with the spin-exchange process and use the appropriate model in Eqs. (11) and (15), i.e., we focus on the $K=0$ case again. The overall model has one nonconserved and one conserved order parameter. The dynamics of the NCOP field $\langle S_k\rangle$ is described by a combination of Eqs. (11) and (25) and the dynamics of the COP field $\langle S_k^2\rangle$ is modeled by Eq. (15). For convenience, we rescale the time scale τ_3, which characterizes spin flips, into the time variable.

We simulate this MF dynamical model on a two-dimensional lattice of size N^2. The details of the simulation and calculated quantities are the same as in Sec. III. The only additional parameter we have here is the ratio τ_3/τ_1, which we set equal to 0.25, so that the frequency of spin exchanges is a quarter of the frequency of spin flips. Because of the rapid domain growth in the case with nonconserved order parameter, we use considerably larger systems here so as to avoid finite-size effects. Thus structure factors and characteristic length scales are computed for systems of size 512^2 as an average over 50 independent runs.

Figure 6 shows evolution pictures for ordering in our MF dynamical model of ferromagnets with annealed vacancies. The vacancy background field is $v_0=0.93$ and the system size is 256^2. As before, regions with positive $\langle S_k\rangle$ (i.e., rich in A or up spins) are marked in black and regions with negative $\langle S_k\rangle$ (i.e., rich in B or down spins) are unmarked. Furthermore, regions where $\langle S_k^2\rangle$ falls below 0.7 (defined as being vacancy rich) are marked by crosses. As in the conserved case, vacancies migrate to the interfacial regions because this

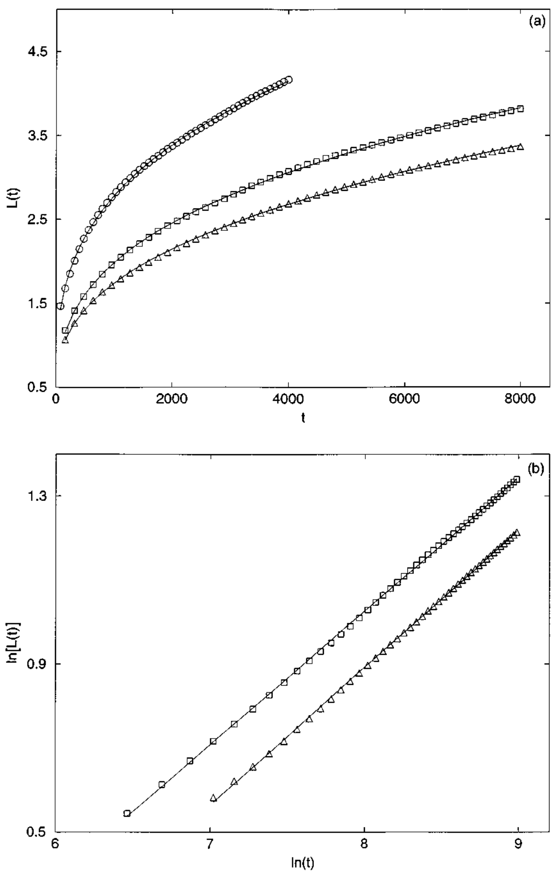

FIG. 5. (a) Characteristic length scale $L(t)$ vs t for the pure case (denoted by $\bigcirc$'s) and the vacancy-driven cases with $v_0=0.93$ (denoted by $\square$'s) and $v_0=0.96$ (denoted by $\triangle$'s). We use a nonlinear fitting routine to fit data to the form $L(t)=a+bt^{\phi}$. The best-fit lines are superposed on the appropriate data sets and the corresponding exponents are as follows: pure case ($\phi=0.33\pm0.01$), $v_0=0.93$ ($\phi=0.34\pm0.01$), and $v_0=0.96$ ($\phi=0.33\pm0.01$). (b) Length scale data for vacancy-driven segregation from (a), plotted on a log-log scale. Symbols have the same meaning as in (a). We have fitted the data to straight lines and these are depicted on the appropriate data sets. The slopes for the best-fit lines are as follows: $v_0=0.93$ ($\phi=0.33\pm0.01$) and $v_0=0.96$ ($\phi=0.32\pm0.01$).

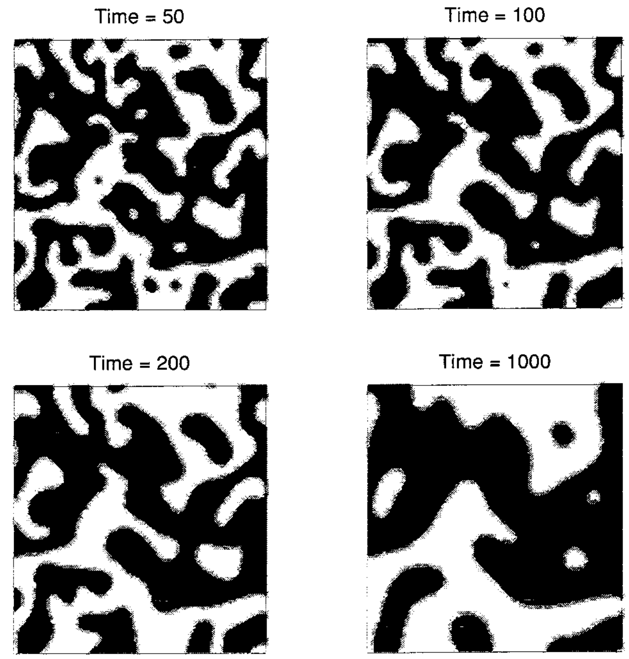

FIG. 6. Temporal evolution from a disordered initial condition for our mean-field dynamical model of ordering in a ferromagnet with annealed vacancies. This model (with $K=0$) is obtained by combining Eq. (11) with Eq. (25) and Eq. (15) with Eq. (26). The other parameter values are $T=0.75T_c$ and $\tau_3/\tau_1=0.25$. The simulation details and our graphic representation are the same as in Fig. 1, except that the system size in this case is 256^2.

is energetically favorable. Figure 7 shows the variation of the order-parameter fields along a horizontal cross section of the evolution pictures in Fig. 6. The solid and dashed lines refer to the $\langle S_k\rangle$ and $\langle S_k^2\rangle$ fields, respectively. Figure 7 demonstrates clearly that there is a surfeit of vacancies in the interfacial regions, as is expected.

Figure 8(a) plots the scaled structure factor $S(k,t)\langle k\rangle^2$ vs $k/\langle k\rangle$ for dimensionless times 400, 600, 800, and 1000. Recall that these data are obtained on 512^2 systems to avoid the possibility of finite-size effects at later times. The quality of scaling is reasonable. Figure 8(b) plots the data of Fig. 8(a) on a log-log scale and demonstrates that the scaling extends into the intermediate tail region. Again, there is an upward drift of the extreme tail, but at a very slow rate. As discussed earlier, this is a possible consequence of the extreme softness of the interfaces resulting from the deposition of vacancies.

Figure 9(a) compares the scaled structure factors for the pure case and the vacancy-affected case with $v_0=0.93$ and 0.96. The agreement is not particularly good, with the scaled structure factor for the pure case exhibiting a sharper falloff than that for the case with vacancies. This difference is highlighted in the log-log plot of Fig. 9(b). Furthermore, scaled structure factors do not agree in the extreme tail regions also. For the pure case, the scaled structure factor has almost reached its asymptotic form in that it exhibits a Porod tail over a large region. However, the extreme tail for the cases with vacancies differs substantially from the Porod tail on the time scales considered.

Finally, Fig. 10 plots the characteristic domain size $L(t)$ vs t for the pure case and the vacancy-affected case with $v_0=0.93$ and 0.96. We have attempted to fit our data to the power-law form $L(t)=a+bt^{\phi}$ using a nonlinear fitting routine. The resultant best fits are denoted by solid lines on the appropriate data sets and the best-fit exponents are specified in the figure caption. These exponents are consistent with the Lifshitz-Cahn-Allen growth law $L(t)\sim a+bt^{1/2}$, which characterizes domain growth in the pure case.

V. SUMMARY AND DISCUSSION

Let us end with a brief summary and discussion of our results in this paper. We initiated this study with two goals in mind. First, we wanted to formulate a coherent phenomenological framework to investigate phase ordering dynamics in ternary mixtures. Monte Carlo models, though relatively easy to formulate, are not particularly useful for investigating the asymptotic behavior of phase ordering dynamics, especially in cases where the ordering field is described by a conserved order parameter. On the other hand, phenomeno-

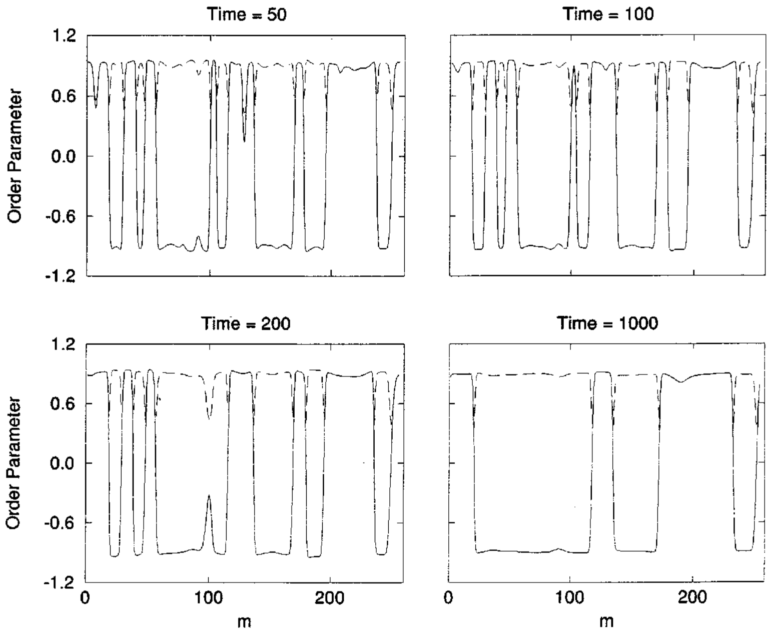

FIG. 7. Order parameter profiles corresponding to the evolution depicted in Fig. 6. The cross section is the same as that in Fig. 2. The solid lines and dashed lines refer to the $\langle S_k \rangle$ and $\langle S_k^2 \rangle$ fields, respectively.

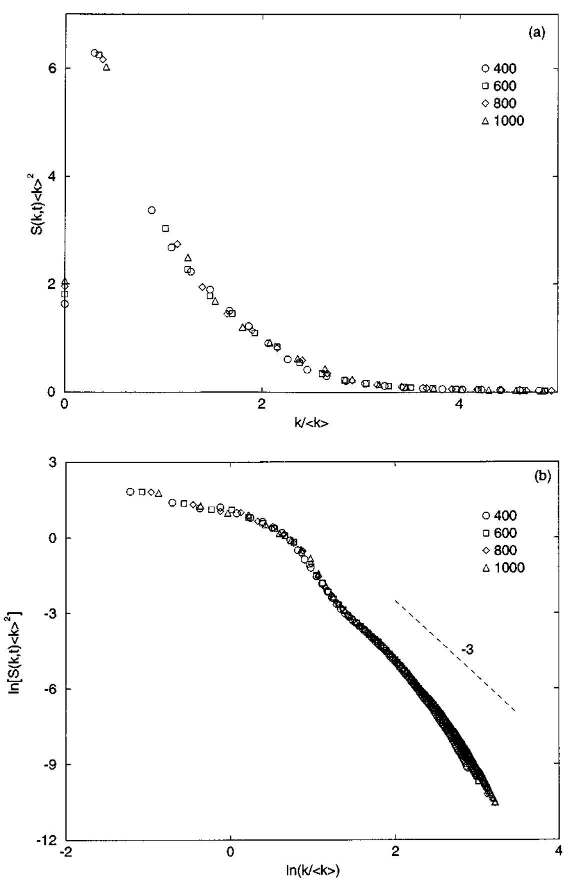

FIG. 8. (a) Scaled structure factors $S(k,t)\langle k \rangle^2$ vs $k/\langle k \rangle$ for the evolution depicted in Fig. 6. Structure factor data are obtained on systems of size 512^2 as an average over 50 independent runs. This figure superposes data from dimensionless times 400, 600, 800, and 1000. (b) Data from (a), plotted on a log-log scale. The dashed line refers to the 2D Porod tail, as in Fig. 3(b).

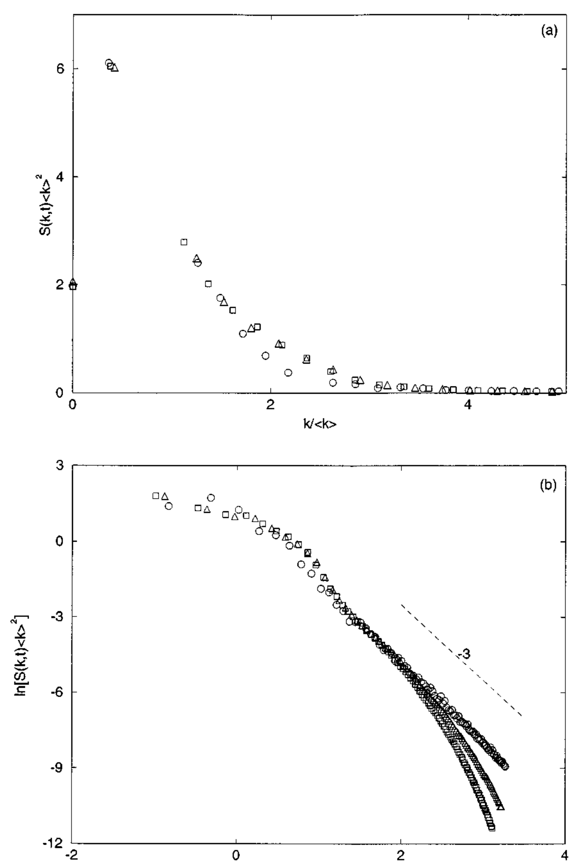

FIG. 9. (a) Analogous to Fig. 4(a), but for the case of ferromagnets with annealed vacancies. All data sets are from dimensionless time 1000. Data for the pure case are denoted by ○'s and for the vacancy-affected cases by □'s (for $v_0 = 0.93$) and △'s (for $v_0 = 0.96$). (b) Data from (a), plotted on a log-log scale. Symbols have the same meaning as in (a). The dashed line refers to the 2D Porod tail.

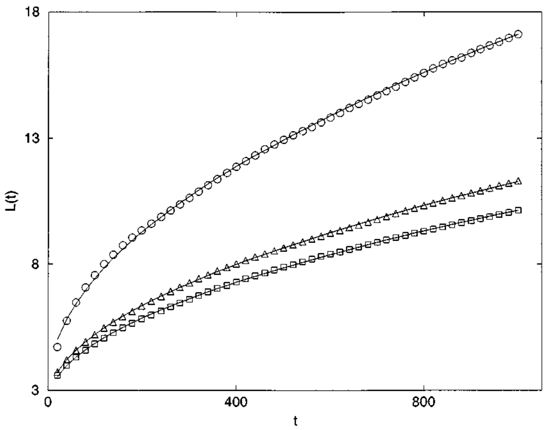

FIG. 10. Analogous to Fig. 5(a), but for the case of ferromagnets with annealed vacancies. The nonlinear best-fit lines are superposed on the appropriate data sets. The corresponding growth exponents are $\phi = 0.51 \pm 0.01$ (for the pure case, denoted by ○'s), $\phi = 0.50 \pm 0.01$ (for $v_0 = 0.93$, denoted by □'s), and $\phi = 0.51 \pm 0.01$ (for $v_0 = 0.96$, denoted by △'s).

logical models have been highly successful in elaborating the asymptotic behavior of phase ordering dynamics, at least for the pure case. It is thus reasonable to expect that the same would also be true for more complicated problems.

We model ternary phase ordering mixtures by an ABV lattice model, where A and B refer to components of a binary alloy in the case with a conserved order parameter, or up and down spins in the case with a nonconserved order parameter. The component V refers to a conserved vacancy field. This ABV model can be rewritten in terms of a spin-1 model with the states $S_i = 1, 0$, and -1 corresponding to A, V, and B, respectively. We associate kinetics with this model and obtain MF dynamical models using a methodology based on the master equation [6]. In all, we consider four different situations that correspond to (a) conserved kinetics in which $\pm 1 \leftrightarrow 0$, (b) nonconserved kinetics in which $\pm 1 \rightarrow 0$ and vice versa, (c) nonconserved kinetics in which $+1 \rightarrow -1$ and vice versa, and (d) conserved kinetics in which $+1 \leftrightarrow -1$.

The resultant MF models are dynamical equations for the order parameters $\langle S_k \rangle$ and $\langle S_k^2 \rangle$, which describe the AB and V fields, respectively. They all contain the correct MF static solution, which is an important check on their reasonableness. Various physical problems involving ABV mixtures can be investigated as combinations of models (a)–(d) above. Furthermore, though we considered only specific interactions that were of relevance to our present study, it should be apparent that our methodology easily extends to the case of ternary mixtures with more general interactions.

We should stress that the approach based on the master equation does not constitute a rigorous derivation of these MF dynamical models. Rather, they are best viewed as phenomenological models and the master equation approach is merely a means of motivating a reasonable phenomenological model. As with all good phenomenology, the true test of these models lies in a comparison with experimental results and numerical results from microscopic MC models.

Our second goal in this paper was to address two important phase ordering problems using these models. The first problem we considered was that of vacancy-mediated spinodal decomposition. Our numerical results for this and the subsequent problem were obtained in a parameter range corresponding to two-phase coexistence. It is generally believed that spinodal decomposition proceeds via vacancy-atom exchanges [18] rather than the Kawasaki spin-exchange kinetics customarily used to model phase separation. Our numerical results demonstrate that vacancy-mediated spinodal decomposition gives rise to domain growth characterized by a length scale $L(t)$, which obeys the Lifshitz-Slyozov growth law $L(t) \sim t^{1/3}$ over the time scales of our simulation.

As far as the scaled structure factor is concerned, vacancy-driven spinodal decomposition is characterized by approximately the same functional form as the usual Kawasaki kinetics. However, there are subtle points of difference, especially in the tail regions. We believe that these differences are nonuniversal effects due to extremely soft vacancy-rich interfaces. We are presently studying this problem in the physically relevant regime where the ABV system shows three-phase coexistence. In this situation, the phase separating system exhibits a time-dependent interfacial thickness due to the ongoing accretion of vacancies at the interface, resulting in a slowing down of the asymptotic domain growth law. Furthermore, in this case, the Porod tail is not recovered even asymptotically because of the growing interfacial width.

The second problem we considered was that of ordering in ferromagnets with annealed vacancies. Again, the results are similar to those obtained for the conserved case. Thus the domain length scale $L(t)$ obeys the Lifshitz-Cahn-Allen law $L(t) \sim t^{1/2}$ over the time scales of our simulation. As far as scaled structure factors are concerned, the functional form for the pure case differs from that for the pure case with vacancies. It is our belief that this is a consequence of strong nonuniversal features introduced by the time-dependent interface thickness. Clearly, longer simulations of larger systems are required before we can make conclusive statements about the apparent differences in the scaled structure factors.

As we have remarked earlier, our modeling in this paper can easily be extended to other ternary mixtures also. It is our hope that the results in this paper will facilitate investigation of the late-stage behavior of phase ordering ternary mixtures in general and ABV models in particular.

ACKNOWLEDGMENTS

S.P. is grateful to K. Binder for suggesting this problem and for many useful discussions. He would also like to thank S. Dattagupta, A. J. Bray, P. Fratzl, J.-F. Gouyet, D. Kumar, J. L. Lebowitz, Y. Oono, and O. Penrose for useful input. Also, he would like to thank P. Fratzl for sending him copies of the Fratzl-Penrose papers cited in Ref. [14(b)]. Finally, he would like to thank Y. Oono for inviting him to Urbana and A. J. Bray for inviting him to Manchester, where most of the numerical work described in the text was done. R.S. gratefully acknowledges financial assistance from CSIR, India through Grant No. 9/263205/92-EMR-I.

[1] For reviews, see J. D. Gunton, M. San Miguel, and P. S. Sahni, in *Phase Transitions and Critical Phenomena*, edited by C. Domb and J. L. Lebowitz (Academic, New York, 1983), Vol. 8, p. 267; K. Binder, in *Materials Science and Technology, Vol. 5: Phase Transformations of Materials*, edited by R. W. Cahn, P. Haasen, and E. J. Kramer (VCH, Weinheim, 1991), p. 405; A. J. Bray, Adv. Phys. **43**, 357 (1994).

[2] K. Binder and D. Stauffer, Phys. Rev. Lett. **33**, 1006 (1974); Z. Phys. B **24**, 406 (1976).

[3] K. Kawasaki, in *Phase Transitions and Critical Phenomena*, edited by C. Domb and M. S. Green (Academic, New York, 1972), Vol. 2, p. 443, and references therein.

[4] J. W. Cahn and H. E. Hilliard, J. Chem. Phys. **28**, 258 (1958).

[5] S. Puri and Y. Oono, J. Phys. A **21**, L755 (1988).

[6] K. Binder, Z. Phys. B **267**, 313 (1974); K. Binder and H. L. Frisch, Z. Phys. B **84**, 403 (1991).

[7] For MC studies with quenched disorder see G. S. Grest and D. J. Srolovitz, Phys. Rev. B **32**, 3014 (1985); D. Chowdhury, M. Grant, and J. D. Gunton, *ibid.* **35**, 6792 (1987); D. Chowdhury and S. Kumar, J. Stat. Phys. **49**, 855 (1987); J. H. Oh and D. I. Choi, Phys. Rev. B **33**, 3448 (1986); A. J. Bray and K. Humayun, J. Phys. A **24**, L1185 (1991).

[8] For coarse-grained studies with quenched disorder see S. Puri, D. Chowdhury, and N. Parekh, J. Phys. A **24**, L1087 (1991); S. Puir and N. Parekh, *ibid.* **25**, 4127 (1992); T. Iwai and H. Hayakawa, J. Phys. Soc. Jpn. **62**, 1583 (1993); H. Hayakawa and T. Iwai, in *Pattern Formation in Complex Dissipative Systems*, edited by S. Kai *et al.* (World Scientific, Singapore, 1992), p. 62; M. F. Gyure, S. T. Harrington, R. Strilka, and H. E. Stanley, Phys. Rev. E (to be published); B. Biswal, S. Puri, and D. Chowdhury, Physica A **229**, 72 (1996).

[9] For coarse-grained studies of the quenched random field problem see E. Oguz, A. Chakrabarti, R. Toral, and J. D. Gunton, Phys. Rev. B **42**, 704 (1990); S. Puri and N. Parekh, J. Phys. A **26**, 2089 (1993).

[10] For MC and hybrid model studies of the COP case with surfactants see reviews by D. Chowdhury, J. Phys.: Condens. Matter **6**, 2435 (1994); T. Kawakatsu, K. Kawasaki, M. Furusaka, H. Okabayashi, and T. Kanaya, *ibid.* **6**, 6385 (1994).

[11] For coarse-grained studies of the COP case with surfactants see (a) M. Laradji, H. Guo, M. Grant, and M. J. Zuckermann, J. Phys. A **24**, L629 (1991); see also **4**, 6715 (1992); (b) R. Ahluwalia and S. Puri, *ibid.* **8**, 227 (1996).

[12] For MC studies of the NCOP case with annealed disorder see D. J. Srolovitz and G. N. Hassold, Phys. Rev. B **35**, 6902 (1987); O. G. Mouritsen, *ibid.* **32**, 1632 (1985); O. G. Mouritsen and P. J. Shah, *ibid.* **40**, 11 445 (1989); P. J. Shah and O. G. Mouritsen, *ibid.* **41**, 7003 (1990); E. Vives and A. Planes, Phys. Rev. Lett. **68**, 812 (1992); Phys. Rev. B **47**, 2557 (1993).

[13] For coarse-grained studies of the NCOP case with annealed disorder see T. Ohta, K. Kawasaki, A. Sato, and Y. Enomoto, Phys. Lett. A **126**, 93 (1987); K. R. Elder, B. Morin, M. Grant, and R. C. Desai, Phys. Rev. B **44**, 6673 (1991).

[14] For MC studies of the COP case with annealed disorder see (a) K. Yaldram and K. Binder, Acta Metall. Mater. **39**, 707 (1991); Z. Phys. B **82**, 405 (1991); J. Stat. Phys. **62**, 161 (1991); (b) P. Fratzl and O. Penrose, Phys. Rev. B **50**, 3477 (1994); **55**, 1 (1997).

[15] M. Plapp and J.-F. Gouyet, Phys. Rev. Lett. **78**, 4970 (1997).

[16] S. Puri, Phys. Rev. E **55**, 1752 (1997).

[17] P. C. Hohenbreg and B. I. Halperin, Rev. Mod. Phys. **49**, 435 (1977).

[18] J. R. Manning, *Diffusion Kinetics for Atoms in Crystals* (Van Nostrand, Princeton 1968); C. P. Flynn, *Point Defects and Diffusion* (Clarendon, Oxford, 1972).

[19] M. Blume, V. J. Emery, and R. B. Griffiths, Phys. Rev. A **4**, 1071 (1971); D. Furman, S. Dattagupta, and R. B. Griffiths, Phys. Rev. B **15**, 441 (1977); M. Kaufmann, R. B. Griffiths, J. M. Yeomans, and M. E. Fisher, Phys. Rev. B **23**, 3448 (1981).

[20] K. Binder (private communication).

[21] For the most comprehensive MC study of phase separation in binary mixtures see J. G. Amar, F. E. Sullivan, and R. D. Mountain, Phys. Rev. B **37**, 196 (1988).

[22] Y. Oono and S. Puri, Phys. Rev. Lett. **58**, 836 (1987); Phys. Rev. A **38**, 434 (1988); S. Puri and Y. Oono, *ibid.* **38**, 1542 (1988); A. Chakrabarti and J. D. Gunton, Phys. Rev. B **37**, 3798 (1988).

[23] T. M. Rogers, K. R. Elder, and R. C. Desai, Phys. Rev. B **37**, 9638 (1988).

[24] N. G. Van Kampen, *Stochastic Processes in Physics and Chemistry* (North-Holland, Amsterdam, 1981).

[25] S. K. Ma, *Modern Theory of Critical Phenomena* (Addison-Wesley, Reading, MA, 1982).

[26] Y. Oono and S. Puri, Mod. Phys. Lett. B **2**, 861 (1988).

[27] G. Porod, in *Small-Angle X-Ray Scattering* edited by O. Glatter and O. Kratky (Academic, New York, 1982).